Atmospheric Research 228 (2019) 77–85

Contents lists available at ScienceDirect

Atmospheric Research

journal homepage: www.elsevier.com/locate/atmosres

A modelling study of the continuous ice formation in an autumnal Arctic mixed-phase cloud case

Shizuo Fu[a], Xin Deng[b], Matthew D. Shupe[c], Huiwen Xue[a,*]

[a] Department of Atmospheric and Oceanic Sciences, School of Physics, Peking University, Beijing, China
[b] College of Crop Science, Fujian Agriculture and Forestry University, Fuzhou, Fujian, China
[c] Cooperative Institute for Research in Environmental Sciences, University of Colorado and NOAA Earth System Research Laboratory, Boulder, CO, USA

ARTICLE INFO

Keywords:
Arctic mixed-phase cloud
Ice formation
Cloud top entrainment
Ice-nucleating particle recycling
Secondary ice production

ABSTRACT

An autumnal Arctic mixed-phase cloud case from the Mixed-Phase Arctic Cloud Experiment is simulated with the Weather Research and Forecasting model with a prognostic ice-nucleating particle (INP) formulation to investigate the mechanisms sustaining the continuous ice formation. When the model is run with only primary ice production (PIP) processes, it needs 100 times the observed INP concentration to reproduce the observations. When a secondary ice production (SIP) process, i.e., droplet shattering when supercooled droplets freeze heterogeneously, is added, the model needs 50 times the observed INP concentration to reproduce the observations. Two factors are found to reduce the INP concentration required to reproduce the observations. First, as the cloud moves over the open ocean, the cloud top rises quickly, resulting in a cloud top entrainment rate of ~3.0 cm s^{-1}, which is 4 times as large as that in previous large-eddy simulations of the same case. More INPs can hence be entrained into the cloud. Second, INPs are recycled when ice crystals are completely sublimated below the cloud base. Sensitivity tests show that INP recycling reduces the required INP concentration by a factor of 4. In addition, offline tests show that another two SIP processes, i.e., droplet shattering when supercooled droplets collect small ice crystals and breakup during ice-ice collision, do not substantially contribute to the ice formation in this case.

1. Introduction

Single-layer Arctic mixed-phase cloud (AMC) is usually composed of a thin mixed-phase layer, which is dominated by supercooled liquid water, and an underlying ice-phase layer (Shupe et al., 2008; Morrison et al., 2012). Due to the presence of the liquid layer, AMCs effectively emit longwave radiation and therefore exert a positive radiative forcing on the surface (Makshtas et al., 1999; Shupe and Intrieri, 2004; Girard et al., 2005; Dong et al., 2010; Du et al., 2011; Sedlar et al., 2012). This positive radiative forcing could accelerate the melting of both land ice (Bennartz et al., 2013; Solomon et al., 2017) and sea ice (Mortin et al., 2016; Huang et al., 2018). Although it has been widely recognized that AMCs play an important role in Arctic climate, many processes occurring in AMCs have not been well understood (Morrison et al., 2012; English et al., 2014; Engström et al., 2014; Chu et al., 2018).

Observations show that ice formation in AMCs can persist for many hours and sometimes for several days (e.g., Shupe et al., 2006; Verlinde et al., 2007; Morrison et al., 2012). However, models usually fail to reproduce the observed ice concentrations when prognostic formulations are used to treat ice-nucleating particles (INPs; Fridlind et al., 2007, 2012; Westbrook and Illingworth, 2013; Fridlind and Ackerman, 2018). In a large-eddy simulation (LES) study of a case from the Mixed-Phase Arctic Cloud Experiment (M-PACE), Fridlind et al. (2007) found that when the INP concentration was set to the observed value, the INPs in the mixed layer were depleted in < 2 h. At later times, the only source of INP was from cloud top entrainment, which was too weak to maintain the ice concentration at the observed value. Their sensitivity test showed that three orders of magnitude more INPs were required to make cloud top entrainment a sufficiently strong source of INP. Studies of the cases from the Beaufort Arctic Storms Experiment (BASE; Fridlind et al., 2007), and the Surface Heat Budget of the Arctic Ocean (SHEBA) campaign (Fridlind et al., 2012) also showed that the observed INP concentration was insufficient for the model to reproduce the observed ice concentration.

Several mechanisms have been proposed to justify an increase of the ice concentration in model simulations with prognostic INP formulations. Avramov et al. (2011) performed an LES study of a case from the Indirect and Semi-direct Aerosol Campaign (ISDAC; McFarquhar et al.,

* Corresponding author.
E-mail address: hxue@pku.edu.cn (H. Xue).

https://doi.org/10.1016/j.atmosres.2019.05.021
Received 5 November 2018; Received in revised form 31 March 2019; Accepted 19 May 2019
Available online 21 May 2019

2011), and found that a reservoir of INPs below the cloud base could provide a prolonged supply of INPs and hence maintain the ice formation. Solomon et al. (2015) simulated the same case and found that INP recycling could substantially increase the ice concentration. Fu and Xue (2017) simulated a similar case and showed that the cooling of the cloud continuously activated low-efficiency INPs and maintained the ice formation. The continuous ice formation sustained by cloud cooling was also supported by the LES study of other cases from ISDAC (Savre and Ekman, 2015). Note that the aforementioned mechanisms were closely related to the ISDAC cases, where the AMCs were decoupled from the surface. In other cases, such as those encountered in the M-PACE, the AMCs were strongly coupled to the surface. The efficacy of the aforementioned mechanisms in coupled cases is not guaranteed. Actually, in a LES study of the M-PACE case, Fridlind et al. (2007) has shown that the INP reservoir below cloud base was consumed in a very short time and could not provide INPs at later times. They also argued that the effect of INP recycling was negligible. On the contrary, Fan et al. (2009) showed that the effect of INP recycling was significant in the M-PACE case. In addition to the aforementioned mechanisms, Morrison et al. (2005) proposed that contact freezing could prolong ice formation when contact nuclei were treated separately from other INPs. In this situation, contact freezing was the dominant mode of ice nucleation. However, some later observational studies suggested that immersion freezing, instead of contact freezing, was the dominant ice nucleation mode in mixed-phase clouds (de Boer et al., 2010, 2011). In addition, in order to adequately resolve the dynamical and microphysical processes, the aforementioned modelling studies generally used a relatively small domain (i.e., ~10 km in the horizontal and ~2 km in the vertical).

Secondary ice production (SIP) processes are also frequently invoked to explain the discrepancy between the low INP concentration and the high ice concentration (e.g., Rangno and Hobbs, 2001; Lawson et al., 2015; Field et al., 2017; Huang et al., 2017; Sullivan et al., 2018). Several SIP processes have been identified. Rime splintering is the process where ice fragments are produced when ice particles collect supercooled liquid droplets (Hallett and Mossop, 1974; Field et al., 2017). Although this process can potentially increase the ice concentration by several orders of magnitude, it occurs only when the temperature is between −8 and −3 °C. Another SIP process is collision breakup, where ice fragments are produced when ice-ice collision occurs (Field et al., 2017). Vardiman (1978) interpreted his experiments of collision breakup in terms of the change in momentum, and formulated a parameterization where the number of ice fragments was a function of the momentum change during the ice-ice collision. Recently, Phillips et al. (2017) interpreted the experiments of Takahashi et al. (1995) in terms of the conservation of energy, and built a parameterization where the collision kinetic energy was the governing parameter. Ice fragments can also be produced when a supercooled droplet freezes (i.e., droplet shattering; Dye and Hobbs, 1967; Lawson et al., 2015; Field et al., 2017). By reviewing previous experiments of droplet shattering, Phillips et al. (2018) showed that the number of ice fragments increased with the size of the freezing droplet, and peaked near −15 °C. Note that the freezing of a supercooled droplet can occur either by heterogeneous nucleation or by collecting a small ice crystal (Phillips et al., 2018).

In this study, we also focus on a case from M-PACE (i.e., flight 10a). This case occurred during a cold air outbreak event, where the cold and dry air from the pack ice moved over the relatively warm open Arctic Ocean, leading to the formation of well-organized cloud streets (Verlinde et al., 2007; Solomon et al., 2009). Observations showed that as the cloud moved downwind, the cloud top rose rapidly (Sethuraman et al., 1986; Hartmann et al., 1997). Later modelling studies showed that the rapid lifting of the cloud top was driven by the strong surface fluxes (Harrington and Olsson, 2001; Gryschka and Raasch, 2005; Liu et al., 2006). As will be shown, the rapid lifting results in a large cloud top entrainment rate and can subsequently increase the amount of INPs entrained into the cloud.

Solomon et al. (2009) used the Weather Research and Forecasting (WRF) model to perform meso-scale simulations of the same case from M-PACE, and conducted extensive comparisons between the simulations and observations. Their results showed that the simulations with a two-moment microphysics scheme (Morrison et al., 2009) well reproduced the organized structure, the radiative properties, and the microphysical properties of the cloud system. It is worth mentioning that a diagnostic INP formulation, instead of a prognostic INP formulation, was used in Solomon et al. (2009).

In this study, we investigate the mechanisms that can increase the ice concentration in the model. We also use the WRF model to conduct simulations of the M-PACE case. We first run the model with only primary ice production (PIP) process, and focus on the role of cloud top entrainment in providing INPs to the AMC. We then run the model with a droplet shattering process, and investigate the effect of droplet shattering processes in increasing ice concentration. In section 2, we describe the case, the model, and the experiment setup. Section 3 presents the results. A discussion is given in Section 4, followed with a summary in section 5.

2. Method

2.1. Observations

The M-PACE took place from September 27 to October 22, 2004 (UTC, the same hereinafter; Verlinde et al., 2007). From October 8 to 13, a high pressure system sat over the pack ice to the northeast of Barrow, Alaska. The cold air moved from the pack ice over the relatively warm open ocean, leading to the formation of a long-lived widespread mixed-phase stratocumulus cloud system. Several flights were made to sample this cloud system. In this study, we focus on flight 10a taking off on October 10. During this flight, the aircraft mainly flew along the coast of Alaska. From 01:10 to 02:00, the aircraft performed several spirals over Barrow to detect the vertical structure of the cloud. The microphysics data collected during this time is used to evaluate the simulation results.

A suite of instruments onboard the aircraft were used to measure the properties of both clouds and aerosols. The instrumentation and the data processing algorithms have been well documented in Verlinde et al. (2007), McFarquhar et al. (2007), and Fridlind et al. (2007). In this study, the observed liquid water content (LWC), droplet concentration, ice water content (IWC), and ice concentration are used. Previous studies pointed out that the measured concentration of small ice crystals was not reliable (McFarquhar et al., 2007). When an ice crystal collides with the probe inlet and breaks up into a number of small ice crystals, the concentration of small ice crystals is artificially increased (Korolev and Isaac, 2005; Korolev et al., 2011). The uncertainty in the determination of the depth of field of small ice crystals also results in uncertainty in the concentration of small ice crystals (Korolev, 2007). Therefore, the concentration of only the ice crystals with diameters > 128 μm is used in this study.

The INP concentration was measured with the continuous flow diffusion chamber (Rogers et al., 2001). Previous studies of the M-PACE case did not distinguish the INPs measured below the cloud top from those measured above the cloud top, and obtained a mean INP concentration of $0.2\,L^{-1}$ (Fridlind et al., 2007; Fan et al., 2009). In this study, we use only the INP data obtained above the cloud top, which is defined as the highest point with LWC > $0.001\,g\,m^{-3}$. For the whole flight 10a, the mean INP concentration above the cloud top is $0.18\,L^{-1}$. In addition, the INP concentration obtained during two preceding flights (flew on October 8 and 9, respectively) are similar to that during flight 10a. Prenni et al. (2007) showed that the INP concentration during M-PACE increased with decreasing temperature when temperature was above −12 °C but remained quasi constant when temperature was lower than −12 °C, meaning that the INPs mainly take

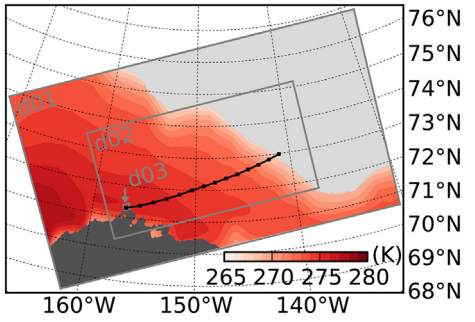

Fig. 1. Domain d01, d02, and d03 are respectively shown with the largest, the medium, and the smallest grey boxes. The light grey region indicates sea ice, and the dark grey region indicates land. The red contours show sea surface temperature of the open ocean. The black line shows a back trajectory in simulation PIP1x, which starts at Barrow at 01:00 October 10. (For interpretation of the references to colour in this figure legend, the reader is referred to the web version of this article.)

effect above −12 °C. At this temperature, the Fletcher parameterization gives an INP concentration of 0.013 L^{-1} (Fletcher, 1962), while the Meyers parameterization gives an INP concentration of 2.6 L^{-1} at water saturation (Meyers et al., 1992).

Data obtained with the ground-based remote sensing instruments, operated by the Atmospheric Radiation Measurement (ARM) Program and located at Barrow (Verlinde et al., 2016), are also used to evaluate the simulation results. Liquid water path (LWP) was retrieved with the microwave radiometer operating at 23.8 and 31.4 GHz, with an uncertainty of 25 g m^{-2} (Shupe et al., 2001, 2005). The ice water path (IWP) was obtained by integrating the IWC, which was calculated based on a power-law relation between IWC and the radar reflectivity measured by the millimeter cloud radar (Shupe et al., 2001, 2005). The estimated uncertainty of IWP is up to 100% (Shupe et al., 2005).

2.2. Model description

The WRF model (version 3.8.1; Skamarock et al., 2008) is used to simulate the M-PACE case. Previous studies found that two-way nesting was generally superior to one-way nesting (Harris and Durran, 2010). We therefore use three two-way nested domains, as shown in Fig. 1. The horizontal resolutions are 6, 1, and 0.2 km for domains d01, d02, and d03, respectively. In order to well resolve the low-level thin cloud system, 30 vertical levels are used in the lowest 1.5 km. The 6-hourly ERA-interim dataset is used for the initial and boundary conditions (Dee et al., 2011). The model runs from 12:00 October 8 to 06:00 October 10. The first 24 h is the spin-up time. The radiative transfer (both longwave and shortwave) is calculated with the RRTMG scheme (Iacono et al., 2008). In all three domains, the boundary layer processes are treated with the YSU scheme (Hong et al., 2006), and the horizontal diffusion is treated with the Smagorinsky first order closure (Skamarock et al., 2008). A discussion of the turbulence in domain d03 and a sensitivity test with 3 dimensional (3D) turbulent kinetic energy (TKE) closure are presented in the Appendix. Microphysical processes are parameterized with the Milbrandt two-moment scheme (Milbrandt and Yau, 2005a, 2005b). In this text, we present only the microphysical processes that are modified. For the other details, please consult the references.

In the original microphysics scheme, PIP processes included contact freezing, deposition nucleation, and condensation nucleation. Contact freezing was parameterized following Young (1974) and Walko et al. (1995). Deposition nucleation and condensation nucleation were not distinguished and were parameterized with the formula from Meyers et al. (1992). Because the Meyers parameterization is a diagnostic relation, it actually provides an unlimited source of INP. Therefore, the original parameterization of ice nucleation does not satisfy the purpose of this study.

In the modified microphysics scheme, the parameterization of contact freezing is retained while the combination of deposition nucleation and condensation nucleation is replaced with immersion freezing. Specifically, two variables are used to represent the INP concentrations. The first represents the concentration of ambient INPs and the second represents the concentration of immersed INPs in liquid droplets. Initially, all INPs are ambient INPs. Ambient INPs are converted to immersed INPs when local saturation ratio over water exceeds one and vertical velocity is > 0.001 m s^{-1}. Immersed INPs are converted back to ambient INPs when local liquid water mixing ratio is smaller than 0.01 g kg^{-1}. Ambient INPs catalyze ice formation through contact freezing, as in the original microphysics scheme. Immersed INPs catalyze ice formation via immersion freezing. Based on this setting, PIP processes mainly occur via immersion freezing. For the INPs entrained from above the cloud top, they are initially ambient INPs, which nucleate ice crystals via contact freezing. However, contact freezing is very slow and produces very few ice crystals. Most ambient INPs are transported downwards. When these ambient INPs are entrained into updrafts, they are converted to immersed INPs, which can then produce significant amount of ice crystals via immersion freezing.

As mentioned above, INPs in the M-PACE case mainly take effect before the temperature becomes lower than −12 °C. We therefore set the nucleating temperature to be −12 °C, i.e., ice nucleation occurs when local temperature is lower than −12 °C. We also require the local liquid water mixing ratio to be > 0.01 g kg^{-1} before immersion freezing can occur. In the M-PACE case, the level of −12 °C is near the cloud base, so PIP processes mainly occur near the cloud base. A sensitivity test with a higher nucleating temperature (−10 °C) produces results similar to the simulation with a nucleating temperature of −12 °C. This is because ice nucleation also occurs near the cloud base in the simulation with a higher nucleating temperature. Another sensitivity test with a lower nucleating temperature (−14 °C) produces less ice than the simulation with a nucleating temperature of −12 °C. In the simulation with a lower nucleating temperature, ice nucleation occurs at a higher elevation so the ice crystals have less time to grow. In this situation, IWC is smaller and the concentration of ice crystals with diameters > 128 μm is lower.

In the original microphysics scheme, rime splintering process is the only SIP process. However, this process does not take effect in the simulated case because the cloud is not in the corresponding temperature range. In the modified scheme, another SIP process, i.e., droplet shattering, is added. Following Phillips et al. (2018), the number of fragments per frozen droplet is parameterized as a function of temperature and droplet size. As mentioned before, droplet shattering can occur either when supercooled droplets freeze heterogeneously or when supercooled droplets collide with smaller ice crystals. In the WRF model, only the first situation is considered. As will be shown, the other situation contributes negligibly to the ice formation in this case. Solid phase hydrometeors are categorized as ice, snow, graupel, and hail in the original microphysics scheme. In this study, graupel and hail are turned off because of their extremely low production rates. Unless specifically mentioned, ice and snow are collectively referred to as ice or ice crystals.

INP recycling is also added to the scheme. When only PIP processes are considered, the complete sublimation of every ice crystal produces an ambient INP. When SIP processes are also considered, some ice crystals do not contain INPs. No INPs should be released when these ice crystals sublimate completely. Therefore, we need to know the fraction of ice crystals that are formed through PIP processes before we can calculate the number of recycled INPs. In every time step, we store the concentration of newly formed ice crystals due to PIP processes and the concentration of newly formed ice crystals due to SIP processes, both of which are averaged over regions of 50 km × 50 km. The mean fraction of newly formed ice crystals due to PIP processes is therefore obtained, and then used to calculate the number of recycled INPs. A sensitivity

test shows that the simulation results are very similar when the averaging region is shrunk from 50 km × 50 km to 20 km × 20 km.

Some other parameters are also modified to be consistent with the observations in the M-PACE case. The relation between mass m (in kg) and diameter D (in m) of an ice crystal is $m = 0.5D^{2.2}$. The relation between the fallspeed v (in m s^{-1}) and D is $v = 45D^{0.6}$ (Fridlind et al., 2007). As in Fridlind et al. (2007), we assume that ice crystals are spherical. In accordance with this assumption, the capacitance C (in m) of ice crystals is set to be $C = 0.5D$ (Pruppacher and Klett, 1997). In addition, the droplet concentration is fixed to the observed value (i.e., 30 cm^{-3}).

2.3. Experiment design

Observations showed that INPs were continuously observed (at least from October 8 to 10), indicating there was a continuous source of INP in the upwind region. In previous LES studies, the INP source was maintained by fixing the INP concentration above the cloud top. In the WRF real case simulation presented here, we fix the INP concentration below 1.5 km over the sea ice, which is indicated with light grey colour in Fig. 1. These INPs are then transported over the open ocean, providing the cloud system with a continuous source of INP.

In this study, the effects of PIP processes and SIP processes are investigated separately. We first run the model with only PIP processes and the observed INP concentration (0.18 L^{-1}). This simulation is called simulation PIP1x. As will be shown, simulation PIP1x produces very few ice crystals. Simulation PIP100x, where the INP concentration is increased to 100 times the observed value, is also run. We then run a simulation with droplet shattering process and 50 times the observed INP concentration. This simulation is called simulation DS50x. Some other sensitivity tests are also performed and are discussed in the appropriate sections.

3. WRF simulation results

3.1. A Lagrangian analysis of cloud evolution

A Lagrangian analysis of cloud evolution is performed by analyzing the cloud properties along back trajectories. The back trajectories are calculated with the horizontal wind at the 20th vertical level (~0.85 km, which is in the middle of the observed cloud). Additionally, the horizontal wind is averaged over a region of 40 km × 40 km to eliminate the effect of small-scale turbulence. The back trajectory starting at Barrow and at 01:00 October 10 in simulation PIP1x is shown with the black line in Fig. 1. The back trajectories in simulations PIP100x and DS50x are very similar to that in simulation PIP1x, provided they start at the same location and the same time.

Fig. 2 shows the evolutions of the LWC profile, IWC profile, and INP concentration profile averaged over regions of 40 km × 40 km along the back trajectories for simulations PIP1x (first row), PIP100x (second row), and DS50x (third row). In all three simulations, the back trajectories start at Barrow and at 01:00 October 10. We first present the results of simulation PIP1x. In this simulation, when the air mass moves over the open ocean, the strong surface fluxes strengthen the turbulence and increase the vapor amount in the boundary layer. Consequently, clouds form about 4 h after the air mass crosses the ice edge (Fig. 2a). At later times, the LWC increases rapidly, along with the cloud top height and cloud base height.

Based on our experimental setup, INPs are released only over the sea ice. They are then efficiently transported over the open ocean and then to the continent (e.g., Barrow; Fig. 2c). After cloud forms, ice nucleation occurs. This leads to the depletion of INPs in the cloud layer (Fig. 2c). However, the INP concentration in simulation PIP1x is so low that the IWC is negligible (Fig. 2b). Because very few ice crystals are available for sublimation, INP recycling is negligible in this simulation.

The fast rising of the cloud top is associated with a large cloud top entrainment rate. Following Moeng (2000), the entrainment rate $w_e = dz_i/dt - w_s$, where z_i is the cloud top height, and w_s is the large-scale subsidence at the cloud top. In this study, cloud top is defined as the highest grid with LWC > 0.001 g m^{-3}. Cloud top height is also averaged over the 40 km × 40 km region, as in the calculation of the averaged wind used to calculate the back trajectories. The large-scale subsidence is averaged over a larger region of 400 km × 400 km. As the air mass moves toward Barrow, the cloud top height increases rapidly (Fig. 3a). The large-scale subsidence first remains nearly constant at -0.2 cm s^{-1}, and then becomes increasingly stronger (Fig. 3b). In simulation PIP1x, the large-scale subsidence is -0.71 cm s^{-1} when the air mass reaches Barrow. This subsidence is close to that in previous studies of the same case, which is approximately -0.7 cm s^{-1} (Fridlind et al., 2007; Klein et al., 2009; Fan et al., 2009). In simulation PIP1x, the entrainment rate is generally larger than 2.0 cm s^{-1} and is 3.2 cm s^{-1} at Barrow (Fig. 3c).

When INP concentration is increased to 100 times the observed value (i.e., simulation PIP100x), much more ice is produced, resulting in a larger IWC (Fig. 2e). Due to the competition between ice crystals and liquid droplets for available water vapor, the growth of ice crystals inhibits the growth of liquid droplets, resulting in a smaller LWC and a higher cloud base (Fig. 2d). The cloud top height and the large-scale subsidence in simulation PIP100x are both similar to those in simulation PIP1x (Fig. 3a and b). Thus, the entrainment rate in simulation PIP100x is also similar to that in simulation PIP1x (Fig. 3c).

INP recycling is important in simulation PIP100x. In this simulation, the ice concentration is relatively high. The competition among ice crystals therefore reduces the growth of ice crystals. In addition, the high cloud base results in a deep sub-saturated layer below cloud base. In response to these two factors, many ice crystals are completely sublimated, leading to the formation of recycled INPs. When the air mass reaches Barrow, the INP concentration below the cloud base is almost the same as that above the cloud top.

The results of the simulation with droplet shattering included and 50 times the observed INP concentration (i.e., DS50x) is shown in the third row in Fig. 2. Compared with simulation PIP100x, simulation DS50x produces slightly higher IWC (Fig. 2h) and slightly less LWC (Fig. 2g). The evolutions of the cloud top height, large-scale subsidence, and entrainment rate in simulation DS50x are almost the same as those in simulation PIP100x (Fig. 3). Additionally, it is found that the amount of recycled INP in simulation DS50x is half of that as in simulation PIP100x (Fig. 2i), indicating that the proportion of INPs that are recycled in simulation DS50x is the same as that in simulation PIP100x.

3.2. Comparison with observations

We now compare the simulation results with the remote sensing and aircraft data to see whether the model can reproduce the observations. All the simulated quantities at Barrow are represented by the values averaged over domain d03. Simulation PIP1x well reproduces the LWP derived from ground-based microwave radiometer (Fig. 4a). In accordance with the LWP, the simulation also reproduces the LWC profile and the droplet concentration profile measured by aircraft (Fig. 5a and b). As mentioned before, this simulation produces very few ice crystals (Fig. 5d), leading to a severe underestimation of IWC (Fig. 5c), and therefore a negligible IWP (Fig. 4b). This result is consistent with previous studies (Fridlind et al., 2007), where the observed INP concentration was found to be too low to reproduce the observed ice concentration.

In simulation PIP100x, the increased INP concentration produces much more ice (Fig. 4b). Nevertheless, the simulated IWP in simulation PIP100x is generally smaller than the retrieved value. Similarly, the simulated LWP is also generally smaller than the retrieved value (Fig. 4a). In our simulation, ice crystals start to form up to 10 h before the air mass reaches Barrow (Figs. 2 and 3). The sedimentation of these ice crystals continuously removes moisture from the air mass, leading to

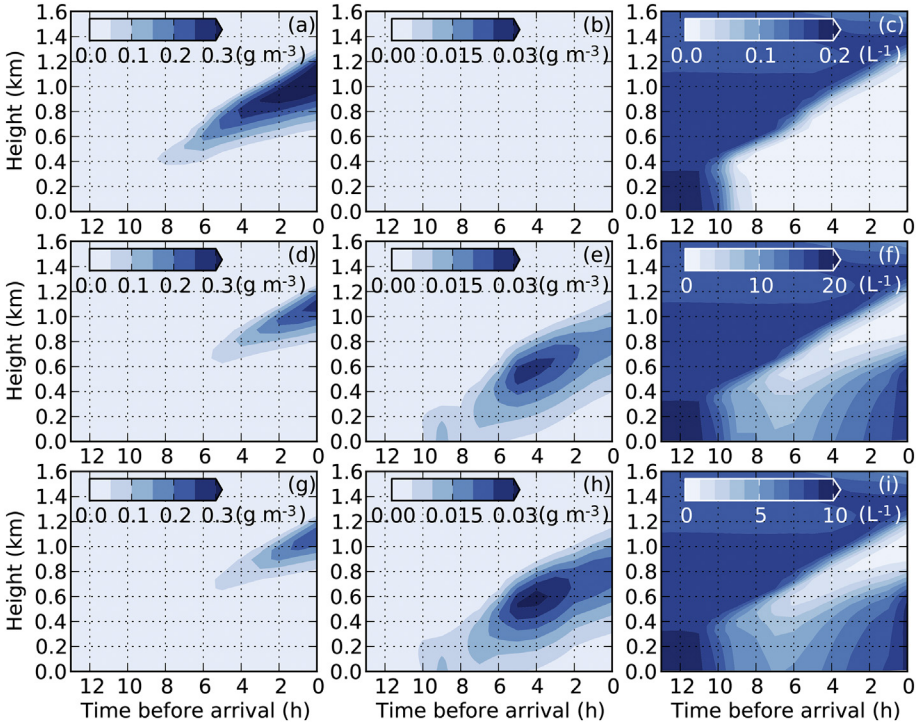

Fig. 2. The evolutions of (left column) LWC profile, (middle column) IWC profile, and (right column) INP concentration profile along the back trajectory starting at Barrow at 01:00 October 10. The first, second, and third rows are respectively for simulations PIP1x, PIP100x, and DS50x. The x-axis shows the time before the back trajectory arrives at Barrow.

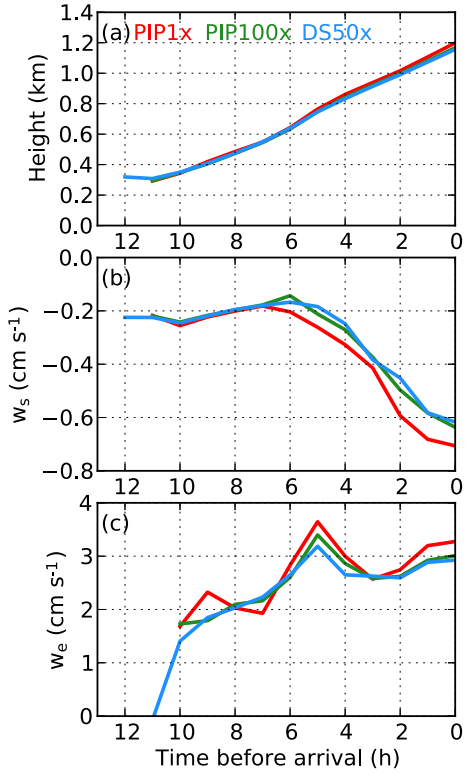

Fig. 3. The evolutions of (a) cloud top height, (b) large-scale subsidence, and (c) entrainment rate along the back trajectories. Simulations PIP1x, PIP100x, and DS50x are shown with red, green, and blue lines, respectively. (For interpretation of the references to colour in this figure legend, the reader is referred to the web version of this article.)

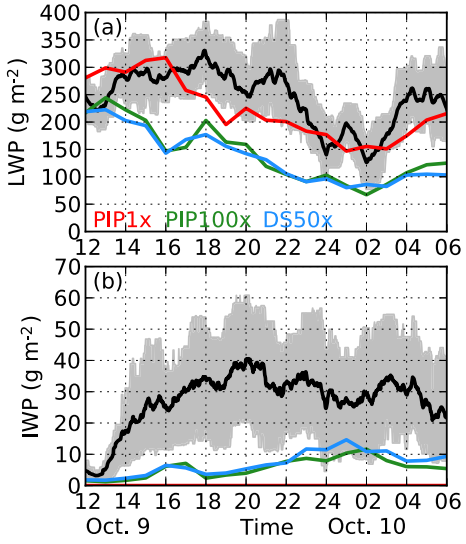

Fig. 4. (a) The simulated and retrieved LWP. Simulations PIP1x, PIP100x, and DS50x are shown with red, green, and blue lines, respectively. The black line shows the 1-hour running mean of the retrieved LWP, and the grey shading indicates the range from 15th to 85th percentile. (b) is the same as (a) but for IWP. (For interpretation of the references to colour in this figure legend, the reader is referred to the web version of this article.)

a small LWP at Barrow. The continuous removal of moisture also reduces the growth of ice crystals, resulting in a small IWP.

From 01:00 to 02:00 on October 10, the simulated IWC profile and ice concentration profile are both close to the aircraft observations (Fig. 5g and h). We note that the simulated IWC is much smaller than the observed value near the cloud top. As mentioned in Section 2.2, ice crystals mainly form near the cloud base. These ice crystals grow rapidly and can hardly reach the cloud top, leading to the underestimation of the IWC near the cloud top. The simulated LWC is slightly smaller than the aircraft observed value (Fig. 5e), consistent with the fact that the simulated LWP is smaller than the retrieved value. In simulation DS50x, the results are almost the same as those in simulation PIP100x (Figs. 4 and 5).

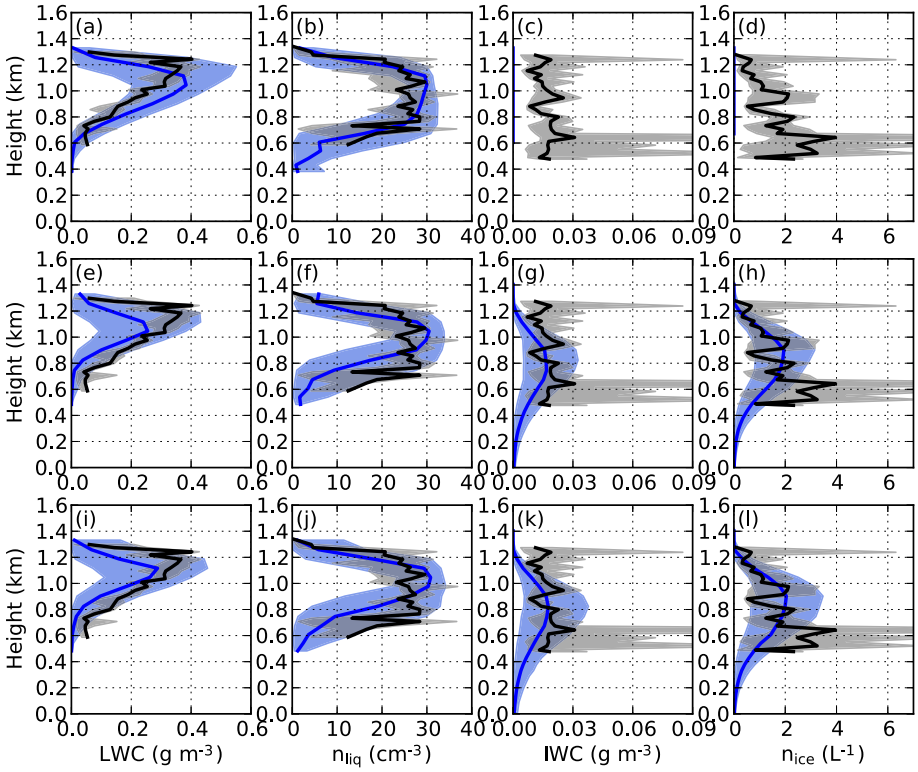

Fig. 5. The simulated (blue) and the aircraft-observed (black) profiles of (first column) LWC, (second column) droplet concentration, (third column) IWC, and (fourth column) concentration of ice crystals with diameters > 128 μm. The first, second, and third rows are for simulations PIP1x, PIP100x, and DS50x, respectively. The solid lines indicate the mean values, and the shadings represent the ranges from 15th to 85th percentile. (For interpretation of the references to colour in this figure legend, the reader is referred to the web version of this article.)

4. Discussion

4.1. Offline calculation of other SIP processes

In the WRF simulations presented, only one SIP process is considered, i.e., droplet shattering when supercooled droplets freeze heterogeneously. Now, we perform offline calculation of another two SIP processes. As has been mentioned, when supercooled droplets collect small ice crystals, they can also produce ice fragments (Phillips et al., 2018). The ice-forming rate due to this process is calculated as a function of rain water content and ice concentration. In this calculation, the rain droplet concentration is fixed at 30 L^{-1}, and the IWC is fixed at 0.02 g m^{-3}, both of which are representative in this case. The temperature is set to −15 °C to maximize the ice-forming rate (Phillips et al., 2018). Fig. 6a shows that the ice-forming rate increases with both the rain water content and the ice concentration. When rain water content becomes larger, the droplets become larger, and can collect more ice crystals, resulting in more ice fragments. When ice concentration increases, more ice crystals can be collected by droplets. In addition, increasing ice concentration also decreases the size of ice crystals. This increases the fall speed difference between droplets and ice crystals, further enhancing the number of ice crystals collected by droplets. In order to evaluate the importance of droplet shattering when supercooled droplets collect ice crystals, we also need to know how often the combination of large rain water content and high ice concentration occurs. Fig. 6b shows the joint distribution of rain water content and ice concentration in domain d03 of simulation PIP100x between 01:00 and 02:00 October 10. It shows that the rain water content is mostly very small. Thus, the contribution of droplet shattering when supercooled droplets collect ice crystals is negligible.

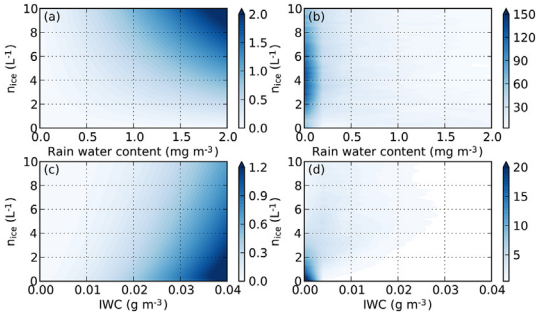

Fig. 6. (a) Ice-forming rate (in L^{-1} h^{-1}) as a function of rain water content and ice concentration for droplet shattering when supercooled droplets collect ice crystals. The rain droplet concentration is fixed at 30 L^{-1}, and the IWC is fixed at 0.02 g m^{-3}. (b) The normalized joint distribution of rain water content and ice concentration in simulation PIP100x between 01:00 and 02:00 October 10. (c) Ice-forming rate as a function of IWC and ice concentration for collision breakup. (d) The same as (b) but for IWC and ice concentration.

The collision breakup process is tested using the momentum based parameterization (Vardiman et al., 1978). In order to maximize the number of fragments produced, the ice crystals are assumed to be the lightly to moderately rimed spatial crystals. Fig. 6c shows that the ice-forming rate due to collision breakup reaches its maximum when IWC is large and ice concentration is low. However, this optimum condition rarely occurs in simulation PIP100x (Fig. 6d), similar to the droplet shattering when supercooled droplets collect small ice crystals.

4.2. INPs emitted from sea surface

Recent studies have pointed out that sea-salt aerosols can be a source of INPs (Burrows et al., 2013; Wilson et al., 2015; DeMott et al., 2016). Here, we briefly show that the INP flux from the sea surface is much smaller than that from cloud top entrainment. Gong (2003) shows that the sea-salt aerosol number flux density can be given by

$$\frac{dF}{dr} = 1.373 u_{10}^{3.41} r^{-A} (1 + 0.057 r^{3.45}) \times 10^{1.607 e^{-B^2}} \quad (1)$$

where r is the radius of sea-salt aerosol (in μm), u_{10} the wind speed at 10 m, $A = 4.7(1 + \Theta r)^{-0.017 r^{-1.44}}$, and $B = (0.433 - logr)/0.433$. The adjustable parameter $\Theta = 30$, as used in Gong (2003). Using Eq. (1), we obtain the total surface area of sea-salt aerosols emitted from the sea

surface. DeMott et al. (2016) gave the surface active site density (n_s) of sea-salt aerosols. The upper bound of n_s at −15 °C, the lowest temperature in the simulated cloud, is approximately 100 cm^{-2}. When we set u_{10} = 12 $m\,s^{-1}$, which is the maximum u_{10} encountered in the simulations, the INP flux is $6 \times 10^3\ m^{-2}\,h^{-1}$. As has be shown, the cloud top entrainment rate is generally > 2.0 $cm\,s^{-1}$, corresponding to an INP flux of $1.3 \times 10^6\ m^{-2}\,h^{-1}$ in simulation PIP100x and $6.5 \times 10^5\ m^{-2}\,h^{-1}$ in simulation DS50x. It can be seen that the INP flux from the sea surface is much weaker than that from the cloud top.

4.3. Comparison with previous studies

The cloud top entrainment rate in this study is much stronger than that in previous studies of the same case. In this study, as revealed by the Lagrangian analysis, the cloud top entrainment rate is ~3.0 $cm\,s^{-1}$ at Barrow. In previous LES studies (Fridlind et al., 2007; Klein et al., 2009; Fan et al., 2009), the cloud top was maintained at quasi-constant heights. This means that the entrainment rate had the same magnitude as the large-scale subsidence, which was ~0.7 $cm\,s^{-1}$. Thus, previous studies underestimated the amount of INPs entrained into the cloud by a factor of 4.

INP recycling is found to play an important role in this study (Fig. 2). Sensitivity tests are performed to further reveal the effect of INP recycling. When INP recycling is neglected, in order to reproduce the observed ice concentration, the INP concentration needs to be 400 times the observed INP concentration in the simulation with only PIP processes, and 200 times the observed INP concentration in the simulation with both PIP and droplet shattering processes. Thus, INP concentration required in the simulations without INP recycling is 4 times that required in the simulations with INP recycling. Fan et al. (2009), who studied the same case as this study, found that the ice concentration in the simulation with INP recycling was 7 times that in the simulation without INP recycling. Solomon et al. (2015), who studies a different case than this study, found that the ice concentration in the simulation with INP recycling was 4 times that in the simulation without INP recycling.

Even when the model has included INP recycling and droplet shattering, and has simulated a stronger cloud top entrainment rate than in previous studies (i.e., simulation DS50x), it still requires 50 times the observed INP concentration to reproduce the observed ice concentration. In previous studies (Fridlind et al., 2007; Fan et al., 2009), several possible mechanisms have been proposed to reproduce the observed ice concentration with the observed INP concentration. For example, evaporating residues become INPs (Beard, 1992), or droplets freeze during evaporation (Cotton and Field, 2002; Durant and Shaw, 2005; Shaw et al., 2005). Due to the lack of reliable parameterizations for these two mechanisms, no further simulation is performed.

5. Summary

An autumnal Arctic mixed-phase cloud case from the M-PACE is simulated with the WRF model to investigate the mechanisms sustaining continuous ice formation. In simulation PIP1x, the model is run with only PIP process and the aircraft-observed INP concentration. It reproduces the observed LWC profile and droplet concentration profile. It also reproduces the observed temporal evolution of LWP. However, this simulation produces very few ice crystals, leading to a severe underestimation of IWC and IWP. The amount of recycled INPs is also negligible in this simulation. In simulation PIP100x, the INP concentration is increased to 100 times the observed value. This simulation reproduces some aspects of the observed IWC, ice concentration, and the temporal evolution of IWP. Due to the higher ice concentration, simulation PIP100x underestimates the LWC and LWP. In this simulation, INP recycling produces an INP reservoir near the surface, which subsequently contributes to ice formation. In simulation DS50x, in addition to PIP processes, the model also has a SIP process, i.e., droplet shattering when supercooled droplets freeze heterogeneously. Additionally, the INP concentration is reduced to 50 times the observed value. The result of simulation DS50x is very similar to that of simulation PIP100x.

In all three simulations, the Lagrangian analysis shows that the cloud top rises quickly as the cloud moves over the open ocean. The fast rising cloud top results in a cloud top entrainment rate of ~3.0 $cm\,s^{-1}$, which is 4 times as large as those in previous studies. As a result, more INPs are entrained into the cloud in this study than in previous studies. In addition, sensitivity tests show that INP recycling can reduce the INP concentration required to reproduce observations by a factor of 4. Offline tests show that another two SIP processes, i.e., droplet shattering when supercooled droplets collect small ice crystals and breakup during ice-ice collision, do not substantially contribute to the ice formation in this case. A simple calculation shows that INPs emitted from the sea surface is also negligible in this case.

While we have identified two mechanisms that can substantially reduce the amount of INPs required by the model to reproduce the observed cloud properties, a significant gap between the low INP concentration and the high ice concentration still exists. In addition, we also find that improving the agreement between the simulated ice concentration and the observed ice concentration reduces the agreement between the simulated LWC and the observed LWC. Information on the spatiotemporal distribution of INPs might be able to bring both the ice phase and the liquid phase closer to observations. In addition, further information on SIP processes are also required to narrow the gap between observations and simulations.

Acknowledgement

We thank Jost Heintzenberg, Fan Yang, Zhiqiang Cui, Lulin Xue, and Aaron Bansemer for their helps. Observational data products were derived from the North Slope of Alaska ground site and research aircraft, both sponsored by the US Department of Energy (DOE) Atmospheric Radiation Measurement (ARM) Program. S. F., X. D., and H. X. were supported by Chinese NSF grants 41675134 and 41330421. M. S. was supported by the DOE Atmospheric System Research Program (DE-SC0011918) and the NOAA Earth System Research Laboratory.

Appendix A

In simulation PIP100x, the TKE production in domain d03 due to buoyancy and shear are very similar to that by Gryschka and Raasch (2005), where very high resolution LES (50 m in the horizontal and 25 m in the vertical) is used to simulate a cold air outbreak event (Fig. A1(a)). The variance of vertical velocity is similar to that observed by Chou et al. (1986), where a cold air outbreak event is observed, and also similar to that simulated by Moeng (1986), where LES of a stratus topped boundary layer is performed (Fig. A1(b)). In our simulations, the TKE in the cloud layer is at least one order of magnitude larger than the variance of vertical velocity (Fig. A1(c)). This is not similar to that in Moeng (1986), where the TKE and the variance of vertical velocity in the cloud layer are of the same order. We are not sure whether this difference is a result of the different cases simulated or the different model setups.

In the sensitivity test, the setups of domains d01 and d02 are the same as that in simulation PIP100x. In domain d03, we turn off the PBL scheme and use the 3D TKE closure to treat diffusion. The results of the sensitivity tests (second row in Fig. A1) are very similar to those of simulation PIP100x, except the magnitude of each quantities is slightly larger. The profiles of LWC, droplet concentration, IWC, and concentration of ice crystals

with diameters > 128 μm in the sensitivity test are all similar to those in simulation PIP100x.

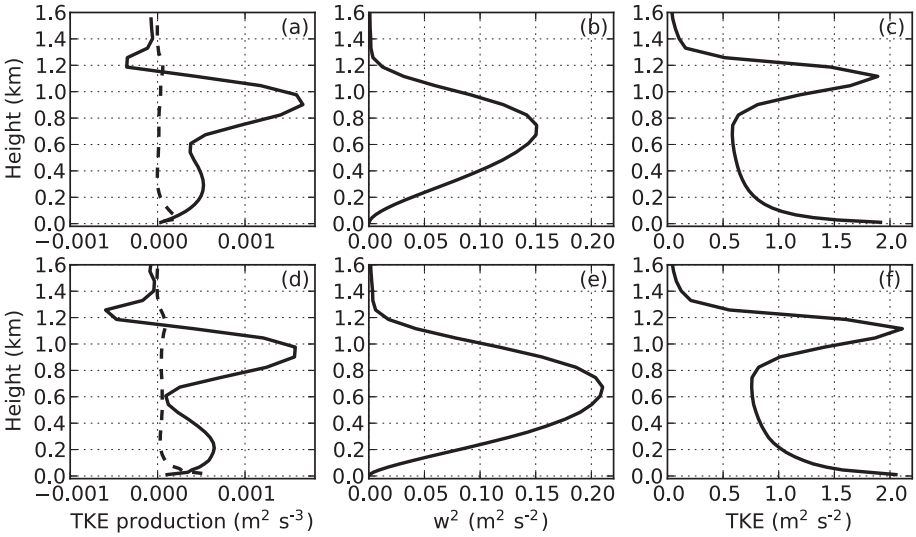

Fig. A1. (a) TKE production due to buoyancy (solid line) and shear (dashed line), (b) variance of vertical velocity, and (c) TKE from simulation PIP100x. (d) (e) and (f) are respectively the same as (a) (b) and (c) but for the sensitivity test (see text for details).

References

Avramov, A., Coauthors, 2011. Toward ice formation closure in Arctic mixed-phase boundary layer clouds during ISDAC. J. Geophys. Res. 116, D00T08. https://doi.org/10.1029/2011JD015910.

Beard, K.V., 1992. Ice initiation in warm-base convective clouds: an assessment of microphysical mechanisms. Atmos. Res. 28, 125–152.

Bennartz, R., Coauthors, 2013. July 2012 Greenland melt extent enhanced by low-level liquid clouds. Nature 496, 83–86. https://doi.org/10.1038/nature12002.

Burrows, S.M., Hoose, C., Pöschl, U., Lawrence, M.G., 2013. Ice nuclei in marine air: biogenic particles or dust? Atmos. Chem. Phys. 13, 245–267. https://doi.org/10.5194/acp-13-245-2013.

Chou, S.-H., Atlas, D., Yeh, E.-N., 1986. Turbulence in a convective marine atmospheric boundary layer. J. Atmos. Sci. 43, 547–564.

Chu, X., Xue, L., Geerts, B., Kosovic, B., 2018. The impact of boundary layer turbulence on snow growth and precipitation: idealized large eddy simulations. Atmos. Res. 204, 54–66. https://doi.org/10.1016/j.atmosres.2018.01.015.

Cotton, R.J., Field, P.R., 2002. Ice nucleation characteristics of an isolated wave cloud. Q. J. R. Meteorol. Soc. 128, 2417–2437.

de Boer, G., Hashino, T., Tripoli, G.J., 2010. Ice nucleation through immersion freezing in mixed-phase stratiform clouds: Theory and numerical simulations. Atmos. Res. 96, 315–324. https://doi.org/10.1016/j.atmosres.2009.09.012.

de Boer, G., Morrison, H., Shupe, M.D., Hildner, R., 2011. Evidence of liquid dependent ice nucleation in high-latitude stratiform clouds from surface remote sensors. Geophys. Res. Lett. 38, L01803. https://doi.org/10.1029/2010GL046016.

Dee, D.P., et al., 2011. The ERA-Interim reanalysis: configuration and performance of the data assimilation system. Q. J. R. Meteorol. Soc. 137, 553–597. https://doi.org/10.1002/qj.828.

DeMott, P.J., et al., 2016. Sea spray aerosol as a unique source of ice nucleating particles. Proc. Natl. Acad. Sci. U. S. A. 113, 5797–5803. https://doi.org/10.1073/pnas.1514034112.

Dong, X., Xi, B., Crosby, K., Long, C.N., Stone, R.S., Shupe, M.D., 2010. A 10 year climatology of Arctic cloud fraction and radiative forcing at Barrow, Alaska. J. Geophys. Res. 115, D17212. https://doi.org/10.1029/2009JD013489.

Du, P., Girard, E., Bertram, A.K., Shupe, M.D., 2011. Modeling of the cloud and radiation processes observed during SHEBA. Atmos. Res. 101, 911–927. https://doi.org/10.1016/j.atmosres.2011.05.018.

Durant, A.J., Shaw, R.A., 2005. Evaporation freezing by contact nucleation inside-out. Geophys. Res. Lett. 32, L20814. https://doi.org/10.1029/2005GL024175.

Dye, J.E., Hobbs, P.V., 1967. The influence of environmental parameters on the freezing and fragmentation of suspended water drops. J. Atmos. Sci. 25, 82–96.

English, J.M., Kay, J.E., Gettelman, A., Liu, X., Wang, Y., Zhang, Y., Chepfer, H., 2014. Contributions of clouds, surface albedos, and mixed-phase ice nucleation schemes to Arctic radiation biases in CAM5. J. Clim. 27, 5174–5197. https://doi.org/10.1175/JCLI-D-13-00608.1.

Engström, A., Karlsson, J., Svensson, G., 2014. The importance of representing mixed-phase clouds for simulating distinctive atmospheric states in the Arctic. J. Clim. 27, 265–272. https://doi.org/10.1175/JCLI-D-13-00271.1.

Fan, J., Ovtchinnikov, M., Comstock, J.M., McFarlane, S.A., Khain, A., 2009. Ice formation in Arctic mixed-phase clouds: Insights from a 3-D cloud-resolving model with size-resolved aerosol and cloud microphysics. J. Geophys. Res. 114, D04205. https://doi.org/10.1029/2008JD010782.

Field, P., co-authors, 2017. Secondary ice production: current state of the science and recommendations for the future. Meteorol. Monogr. 58 (Chapter 7), 7.1–7.19. https://doi.org/10.1175/AMSMONOGRAPHS-D-16-0014.1.

Fletcher, N.H., 1962. Physics of Rain Clouds. vol. 386 Cambridge University Press.

Fridlind, A.M., Ackerman, A.S., 2018. Simulations of Arctic mixed-phase boundary layer clouds: advances in understanding and outstanding questions. In: Andronache, C. (Ed.), Mixed-Phase Clouds: Observations and Modeling. Elsevier Inc, Amsterdam, pp. 153–183.

Fridlind, A.M., Ackerman, A.S., McFarquhar, G., Zhang, G., Poellot, M.R., DeMott, P.J., Prenni, A.J., Heymsfield, A.J., 2007. Ice properties of single-layer stratocumulus during the mixed-phase Arctic Cloud Experiment. Part II: model results. J. Geophys. Res. 112, D24202. https://doi.org/10.1029/2007JD008646.

Fridlind, A.M., van Diedenhoven, B., Ackerman, A.S., Avramov, A., Mrowiec, A., Morrison, H., Zuidema, P., Shupe, M.D., 2012. A FIRE-ACE/SHEBA case study of mixed-phase Arctic boundary layer clouds: entrainment rate limitations on rapid primary ice nucleation processes. J. Atmos. Sci. 69, 365–389. https://doi.org/10.1175/JAS-D-11-052.1.

Fu, S., Xue, H., 2017. The effect of ice nuclei efficiency on Arctic mixed-phase clouds from large-eddy simulations. J. Atmos. Sci. 74, 3901–3913. https://doi.org/10.1175/JAS-D-17-0112.1.

Girard, E., Blanchet, J.-P., Dubois, Y., 2005. Effects of arctic sulphuric acid aerosols on wintertime low-level atmospheric ice crystals, humidity and temperature at alert, Nunavut. Atmos. Res. 73, 131–148. https://doi.org/10.1016/j.atmosres.2004.08.002.

Gong, S.L., 2003. A parameterization of sea-salt aerosol source function for sub- and super-micron particles. Glob. Biogeochem. Cycles 17, 1097.

Gryschka, M., Raasch, S., 2005. Roll convection during a cold air outbreak: a large eddy simulation with stationary model domain. Geophys. Res. Lett. 32, L14805. https://doi.org/10.1029/2005GL022872.

Hallett, J., Mossop, S.C., 1974. Production of secondary ice particles during the riming process. Nature 249, 26–28.

Harrington, J.Y., Olsson, P.Q., 2001. On the potential influence of ice nuclei on surface-forced marine stratocumulus cloud dynamics. J. Geophys. Res. 106, 27 473–27 484. https://doi.org/10.1029/2000JD000236.

Harris, L.M., Durran, D.R., 2010. An idealized comparison of one-way and two-way grid nesting. Mon. Weather Rev. 138, 2174–2187. https://doi.org/10.1175/2010MWR3080.1.

Hartmann, J., Kottmeier, C., Raasch, S., 1997. Roll vortices and boundary-layer development during a cold air outbreak. Bound. Layer Meterol. 84, 45–65.

Hong, S.-Y., Noh, Y., Dudhia, J., 2006. A new vertical diffusion package with an explicit treatment of entrainment processes. Mon. Weather Rev. 134, 2318–2341.

Huang, Y., Blyth, A.M., Brown, P.R.A., Choularton, T.W., Cui, Z., 2017. Factors controlling secondary ice production in cumulus clouds. Q. J. R. Meteorol. Soc. 143, 1021–1031. https://doi.org/10.1002/qj.2987.

Huang, Y., Dong, X., Xi, B., Deng, Y., 2018. A survey of the atmospheric physical processes key to the onset of Arctic sea ice melt in spring. Cim. Dyn. 52, 4907–4922. https://doi.org/10.1007/s00382-018-4422-x.

Iacono, M.J., Delamere, J.S., Mlawer, E.J., Shephard, M.W., Clough, S.A., Collins, W.D., 2008. Radiative forcing by long-lived greenhouse gases: calculations with the AER radiative transfer models. J. Geophys. Res. 113, D13103. https://doi.org/10.1029/2008JD009944.

Klein, S.A., et al., 2009. Intercomparison of model simulations of mixed-phase clouds observed during the ARM Mixed-phase Arctic Cloud Experiment. I: single-layer cloud.

Q. J. R. Meteorol. Soc. 135, 979–1002. https://doi.org/10.1002/qj.416.
Korolev, A., 2007. Reconstruction of the sizes of spherical particles from their shadow images. Part I: theoretical considerations. J. Atmos. Ocean. Technol. 24, 376–389. https://doi.org/10.1175/JTECH1980.1.
Korolev, A., Isaac, G.A., 2005. Shattering during sampling by OAPs and HVPS. Part I: snow particles. J. Atmos. Ocean. Technol. 22, 528–542.
Korolev, A., Emery, E.F., Strapp, J.W., Cober, S.G., Isaac, G.A., Wasey, M., 2011. Small ice particle in tropospheric clouds: Fact or artifact? Airborne icing instrumentation evaluation experiment. Bull. Amer. Meteor. Soc. 92, 967–973. https://doi.org/10.1175/2010BAMS3141.1.
Lawson, R.P., Woods, S., Morrison, H., 2015. The microphysics of ice and precipitation development in tropical cumulus clouds. J. Atmos. Sci. 72, 2429–2445. https://doi.org/10.1175/JAS-D-14-0274.1.
Liu, A.Q., Moore, G.W.K., Tsuboki, K., Renfrew, I.A., 2006. The effect of the sea-ice zone on the development of boundary-layer roll clouds during cold air outbreaks. Bound. Layer Meterol. 118, 557–581. https://doi.org/10.1007/s10546-005-6434-4.
Makshtas, A.P., Andreas, E.L., Svyashchennikov, P.N., Timachev, V.F., 1999. Accounting for clouds in sea ice models. Atmos. Res. 52, 77–113.
McFarquhar, G.M., Zhang, G., Poellot, M.R., Kok, G.L., McCoy, R., Tooman, T., Fridlind, A., Heymsfield, A.J., 2007. Ice properties of single-layer stratocumulus during the mixed-phase Arctic cloud experiment: 1. observations. J. Geophys. Res. 112, D24201. https://doi.org/10.1029/2007JD008633.
McFarquhar, G.M., et al., 2011. Indirect and semi-direct aerosol campaign (ISDAC): the impact of Arctic aerosols on clouds. Bull. Am. Meteorol. Soc. 92, 183–201. https://doi.org/10.1175/2010BAMS2935.1.
Meyers, M.P., Demott, P.J., Cotton, W.R., 1992. New primary ice nucleation parameterizations in an explicit cloud model. J. Appl. Meteorol. 31, 708–721.
Milbrandt, J.A., Yau, M.K., 2005a. A multimoment bulk microphysics parameterization. Part I: analysis of the role of the spectral shape parameter. J. Atmos. Sci. 62, 3051–3064.
Milbrandt, J.A., Yau, M.K., 2005b. A multimoment bulk microphysics parameterization. Part II: a proposed three moment closure and scheme description. J. Atmos. Sci. 62, 3065–3081.
Moeng, C.-H., 1986. Large-eddy simulation of a stratus-topped boundary layer. Part I: structure and budgets. J. Atmos. Sci. 43, 2886–2900.
Moeng, C.-H., 2000. Entrainment rate, cloud fraction, and liquid water path of PBL stratocumulus clouds. J. Atmos. Sci. 57, 3627–3643.
Morrison, H., Shupe, M.D., Pinto, J.O., Curry, J.A., 2005. Possible roles of ice nucleation mode and ice nuclei depletion in the extended lifetime of Arctic mixed-phase clouds. Geophys. Res. Lett. 32, L18801. https://doi.org/10.1029/2005GL023614.
Morrison, H., Thompson, G., Tatarskii, V., 2009. Impact of cloud microphysics on the development of trailing stratiform precipitation in a simulated squall line: Comparison of one- and two-moment schemes. Mon. Weather Rev. 137, 991–1007. https://doi.org/10.1175/2008MWR2556.1.
Morrison, H., de Boer, G., Feingold, G., Harrington, J., Shupe, M.D., Sulia, K., 2012. Resilience of persistent Arctic mixed-phase clouds. Nat. Geosci. 5, 11–17. https://doi.org/10.1038/ngeo1332.
Mortin, J., Svensson, G., Graversen, R.G., Kapsch, M.-L., Stroeve, J.C., Boisvert, L.N., 2016. Melt onset over Arctic sea ice controlled by atmospheric moisture transport. Geophys. Res. Lett. 43, 6636–6642. https://doi.org/10.1002/2016GL069330.
Phillips, V.T.J., Yano, J.-I., Khain, A., 2017. Ice multiplication by breakup in ice–ice collisions. Part I: theoretical formulation. J. Atmos. Sci. 74, 1705–1719. https://doi.org/10.1175/JAS-D-16-0224.1.
Phillips, V., Patade, S., Gutierrez, J., Bansemer, A., 2018. Secondary ice production by fragmentation of freezing drops: formulation and theory. J. Atmos. Sci. 75, 3031–3070. https://doi.org/10.1175/JAS-D-17-0190.1.
Prenni, A.J., et al., 2007. Can ice-nucleating aerosols affect Arctic seasonal climate? Bull. Am. Meteorol. Soc. 88, 541–550. https://doi.org/10.1175/BAMS-88-4-541.
Pruppacher, H.R., Klett, J.D., 1997. Microphysics of Clouds and Precipitation, 2nd ed. vol. 954 Kluwer Academic Publishers.
Rangno, A.L., Hobbs, P.V., 2001. Ice particle in stratiform clouds in the Arctic and possible mechanisms for the production of high ice concentrations. J. Geophys. Res. 106, 15,065–15,075.
Rogers, D.C., DeMott, P.J., Kreidenweis, S.M., Chen, Y., 2001. A continuous-flow diffusion chamber for airborne measurements of ice nuclei. J. Atmos. Ocean. Technol. 18, 725–741.
Savre, J., Ekman, A.M.L., 2015. Large-eddy simulation of three mixed-phase cloud events during ISDAC: Conditions for persistent heterogeneous ice formation. J. Geophys. Res. Atmos. 120, 7699–7725. https://doi.org/10.1002/2014JD023006.
Sedlar, J., Shupe, M.D., Tjernström, M., 2012. On the relationship between thermodynamic structure and cloud top, and its climate significance in the Arctic. J. Clim. 25, 2374–2393. https://doi.org/10.1175/JCLI-D-11-00186.1.
Sethuraman, S., Riordan, A.J., Holt, T., Stunder, M., Hinman, J., 1986. Observations of the marine boundary layer thermal structure over the Gulf Stream during a cold air outbreak. J. Clim. Appl. Meteorol. 25, 14–21.
Shaw, R.A., Durrant, A., Mi, Y., 2005. Heterogeneous Surface Crystallization Observed in Undercooled Water. J. Phys. Chem. 109, 9865–9868. https://doi.org/10.1021/jp0506336.
Shupe, M.D., Intrieri, J.M., 2004. Cloud radiative forcing of the Arctic surface: the influence of cloud properties, surface albedo, and solar zenith angle. J. Clim. 17, 616–628.
Shupe, M.D., Uttal, T., Matrosov, S.Y., Frisch, A.S., 2001. Cloud water contents and hydrometeor sizes during the FIRE Arctic clouds experiment. J. Geophys. Res. 106, 15015–15028.
Shupe, M.D., Uttal, T., Matrosov, S.Y., 2005. Arctic cloud microphysics retrievals from surface-based remote sensors at SHEBA. J. Appl. Meteorol. 44, 1544–1562.
Shupe, M.D., Matrosov, S.Y., Uttal, T., 2006. Arctic mixed-phase cloud properties derived from surface-based sensors at SHEBA. J. Atmos. Sci. 63, 697–711. https://doi.org/10.1175/JAS3659.1.
Shupe, M., Kollias, P., Persson, P.O.G., McFarquhar, G.M., 2008. Vertical motions in Arctic mixed-phase stratus. J. Atmos. Sci. 65, 1304–1322. https://doi.org/10.1175/2007JAS2479.1.
Skamarock, W.C., Klemp, J.B., Dudhia, J., Gill, D.O., Barker, D.M., Duda, M.G., Huang, X.-Y., Wang, W., Powers, J.G., 2008. A Description of the Advanced Research wrf version 3. Ncar Technical Note 475.
Solomon, A., Morrison, H., Persson, O., Shupe, M., Bao, J.-W., 2009. Investigation of microphysical parameterizations of snow and ice in Arctic clouds during M-PACE through model–observation Comparisons. Mon. Weather Rev. 137, 3110–3128. https://doi.org/10.1175/2009MWR2688.1.
Solomon, A., Feingold, G., Shupe, M.D., 2015. The role of ice nuclei recycling in the maintenance of cloud ice in Arctic mixed-phase stratocumulus. Atmos. Chem. Phys. 15 (10), 631–10 643. https://doi.org/10.5194/acp-15-10631-2015.
Solomon, A., Shupe, M.D., Miller, N.B., 2017. Cloud–atmospheric boundary layer–surface interactions on the Greenland ice sheet during the July 2012 extreme melt event. J. Clim. 30, 3237–3252. https://doi.org/10.1175/JCLI-D-16-0071.1.
Sullivan, S.C., Hoose, C., Kiselev, A., Leisner, T., Nenes, A., 2018. Initiation of secondary ice production in clouds. Atmos. Chem. Phys. 18, 1593–1610. https://doi.org/10.5194/acp-18-1593-2018.
Takahashi, T., Nagao, Y., Kushiyama, Y., 1995. Possible high ice particle production during graupel–graupel collisions. J. Atmos. Sci. 52, 4523–4527.
Vardiman, L., 1978. The generation of secondary ice particles in clouds by crystal–crystal collision. J. Atmos. Sci. 35, 2168–2180.
Verlinde, J., Coauthors, 2007. The mixed-phase Arctic Cloud Experiment. Bull. Amer. Meteor. Soc. 88, 205–221. https://doi.org/10.1175/BAMS-88-2-205.
Verlinde, J., Zak, B.D., Shupe, M.D., Ivey, M.D., Stamnes, K., 2016. The ARM north slope of Alaska (NSA) sites. Meteorol. Monogr. 57 (Chapter 8), 8.1–8.13. https://doi.org/10.1175/AMSMONOGRAPHS-D-15-0023.1.
Walko, R.L., Cotton, W.R., Meyers, M.P., Harrington, J.Y., 1995. New RAMS cloud microphysics. Part I: the one moment scheme. Atmos. Res. 38, 29–62.
Westbrook, C.D., Illingworth, A.J., 2013. The formation of ice in a long-lived supercooled layer cloud. Quart. J. Roy. Meteor. Soc. 139, 2209–2221. https://doi.org/10.1002/qj.2096.
Wilson, T.W., et al., 2015. A marine biogenic source of atmospheric ice-nucleating particles. Nature 525, 234–238. https://doi.org/10.1038/nature14986.
Young, K.C., 1974. The role of contact nucleation in ice phase initiation in clouds. J. Atmos. Sci. 31, 1735–1748.